Proceedings of the 9th International and 49th National Conference on Fluid Mechanics and Fluid Power (FMFP)
December 14-16, 2022, IIT Roorkee, Roorkee-247667, Uttarakhand, India

FMFP2022–3868

CFD Investigations on a Pitch Type Wave Energy Converter for a Potential Site along the Indian Coast

Achanta V. V. D. Pavan [1], Anup P. Kamath[1], Dhanush Binu[1], Siddharthkumar B. Zadafiya[1], and Jyotirmay Banerjee[1]

[1]Department of Mechanical Engineering, S.V. National Institute of Technology, Surat-395007, India

ABSTRACT

The objective of the present work is to assess the performance of a pitch type WEC suited for a potential location along the Indian coastline through CFD simulations of multiphase flows. A numerical wave tank (NWT) is modelled and validated with and without the presence of the WEC-rotor, with the waves being generated by the inlet velocity using Stokes second-order wave theory. Based on the hydrodynamic performance assessment carried out, the power absorption capacity and hydrodynamic efficacy of the WEC- rotor is estimated for a range of sea-states.

Keywords: Renewable energy, Ocean wave energy harnessing, Pitch type WEC, CFD simulations, Stokes second-order wave theory

1. Introduction

India is estimated to have a wave potential of 60000 MW, out of which around 6000 MW is exploitable by means of wave energy harnessing devices, having considered the site constraints and energy losses [1]. Unlike other renewable energy resources, ocean wave energy is highly predictable, owing to its propagation throughout. Ocean waves are found to have much higher energy densities compared to other alternative energy resources. With regard to the Indian scenario, energy from waves can be well tapped from coasts of Gujarat, Maharashtra, Karnataka, Kerala, Tamil Nadu, and Andhra Pradesh. It is important to consider the variability of wave power while selecting a site.

Wave resource in India is found to be richer in the western coast when compared to the eastern coast. Due to the strong winds from the east African mountains, the annual wave activity in the western coast is more enhanced. These winds help in strengthening the harsh oceanic circulation hence the heat received at the surface is transported southward and into the deeper ocean. The wave activity in the western coast is determined by the monsoon winds which occur during June to September and Shamal winds, which are the seasonal winds that occur during November to March and from June to August. In contrary, the eastern coast experiences high cyclone frequency which describes the majority wave climate in this region. Extreme waves occur frequently in the eastern coast of India during the northeast monsoon season that impacts the life span of WECs. The uncertainties involved with such unprecedented natural occurrences require a critical analysis to account for the WEC safety.

The present study is divided as follows: Section 2 discusses bases for the wave resource assessment, which forms an integral part of site selection. Section 3 involves a quantitative approach towards site selection. Section 4 covers modelling and simulation of a NWT with and without a single degree of freedom pitch type WEC-rotor. The response of rotor is validated against the results of Poguluri et al. [2], which is further used for the performance assessment. Subsequently, Section 5 is focussed on the hydrodynamic performance study of the pitch type WEC-rotor for the selected site. A comparison has been carried out for a range of sea-states, with key parameters such as power absorption capacity, hydrodynamic efficiency, etc. determined. Section 6 and 7 enunciate key results and conclusions drawn from the study respectively.

2. Selection of site

The selection of site suited for an optimal wave energy harnessing mechanism is a prime step towards ensuring an efficient exploitation of the available wave energy resource. Various methodologies have been studied to uniformly contrast operation sites based on the wave information acquired. Three such methods have been described, highlighting the pre-requisite input data and the computation of indices which denote the suitability of the site under consideration. The Geographic Information System (GIS) holds worthy to compare potential sites for WEC deployment. It involves gathering of site specific details such as wave energy resource, availability of grid, proximity to energy consumers, pre-installed infrastructure and interference with biological activities. Having weighted these factors, the GIS tool is integrated to determine the ideal site with minimal constraints. Lavidas George [3] proposed the Selection Index for Wave Energy Deployment (SIWED) that takes parameters pertaining to harnessing device as well as the location of interest into consideration. The SIWED approach requires wave data over a thirty-year period for an analysis of extreme events. The index is expressed as follows:

$$SIWED = \frac{e^{-CoV.CF}}{(\frac{H_{EVA}}{H_{max}})} \tag{1}$$

Kamranzad et al. [4] suggested adoption of Optimum Hotspot Identifier (OHI) to select a suitable site. This simplistic approach considers three factors for comparison namely, local mean wave power flux, temporal variability in waves and frequency of exploitable power occurrence. Temporal variability indicates the variation of wave power over a specified time period. Trivially, a location with a higher variability index shall not be reliable for deployment.

$$OHI = \frac{P_{mean} \cdot F_{mean}}{MVI} \tag{2}$$

A few prospective locations along the western coastline of India have been analyzed based on oceanic information from ESSO-INCOIS so as to determine an optimal site for which a WEC can be deployed. The sites of interest (stations) analyzed are namely, Veraval, Ratnagiri, Karwar and Kollam. Through the OHI approach, the respective indices have been compared for each of these stations to take into account the trends in the local wave behaviour. Primarily, the wave power (P_w), which is a function of significant wave height and wave energy period, is computed as mentioned below [4].

$$P_w = \frac{\rho g^2 H_s^2 T_e}{64\pi} \tag{3}$$

It is stated that absorbed wave power greater than 2 kW/m improves capacity factor and the power produced, and hence is termed to be the exploitable wave power [5]. F_{mean} is thus determined by making use of an appropriate distribution to fit the wave power data so as to calculate the probability of exploitable wave power occurrence.

$$F_{mean} = P(P_w > 2\ kW/m) \tag{4}$$

Table 1: Comparison of OHI for the selected locations

Station	$P_{m,max}$	$P_{m,min}$	P_{mean}	MVI	F_{mean}	OHI
Veraval	24.807	1.486	6.538	3.567	57.97	1.0626
Ratnagiri	24.675	1.320	6.462	3.614	62.81	1.1 230
Karwar	27.502	1.531	8.927	2.909	58.27	1.7 881
Kollam	13.811	0.957	5.037	2.552	63.02	1.2 439

Temporal variability index on a seasonal or annual basis is essential to take into account, the fluctuations in wave power levels over the specified period of time. Monthly Variability Index (MVI) is calculated for the stations to obtain the variability on an intra-annual basis for one year period, i.e., April 2020 to March 2021 based on the oceanic data retrieved. The *MVI* is computed using the equation below [4].

$$MVI = \frac{P_{m,max} - P_{m,min}}{P_{mean}} \tag{5}$$

Using Equation 2, the OHI for the station can be solved and the results have been summarized in Table 1. It can be well observed that Karwar possessing a relatively higher OHI shall be considered as a potential site for WEC deployment.

3. Theoretical aspects

The CFD simulations for ocean waves employ the numerical solutions of the Navier-Stokes equations and other accompanying equations. Some of the key theoretical aspects supporting the study are discussed herewith.

3.1. Navier-Stokes equations

The Navier-Stokes equations for an incompressible, inviscid fluid flow are the fundamental equations required to be solved for momentum and pressure fields. These are represented in Cartesian coordinates as depicted below,

$$\begin{aligned}
\rho\left(\frac{\partial u}{\partial t} + u\frac{\partial u}{\partial x} + v\frac{\partial u}{\partial y} + w\frac{\partial u}{\partial z}\right) &= -\frac{\partial p}{\partial x} + \mu\left(\frac{\partial^2 u}{\partial x^2} + \frac{\partial^2 u}{\partial y^2} + \frac{\partial^2 u}{\partial z^2}\right) + \rho g_x \\
\rho\left(\frac{\partial v}{\partial t} + u\frac{\partial v}{\partial x} + v\frac{\partial v}{\partial y} + w\frac{\partial v}{\partial z}\right) &= -\frac{\partial p}{\partial y} + \mu\left(\frac{\partial^2 v}{\partial x^2} + \frac{\partial^2 v}{\partial y^2} + \frac{\partial^2 v}{\partial z^2}\right) + \rho g_y \\
\rho\left(\frac{\partial w}{\partial t} + u\frac{\partial w}{\partial x} + v\frac{\partial w}{\partial y} + w\frac{\partial w}{\partial z}\right) &= -\frac{\partial p}{\partial z} + \mu\left(\frac{\partial^2 w}{\partial x^2} + \frac{\partial^2 w}{\partial y^2} + \frac{\partial^2 w}{\partial z^2}\right) + \rho g_z
\end{aligned} \tag{6}$$

where, ρ is the density of the fluid mixture in kg/m^3, p is the pressure in Pa, g is the acceleration due to gravity in m/s^2, μ is the dynamic viscosity of fluid in Pa.s, t represents the time and u, v, w denote the velocity components in x, y and z directions respectively.

With the flow being considered incompressible, the continuity equation must be obeyed as follows,

$$\frac{\partial u}{\partial x} + \frac{\partial v}{\partial y} + \frac{\partial w}{\partial z} = 0 \tag{7}$$

3.2. Volume of Fluids (VOF) model

Tracking the movement of the air-water interface requires the Volume of Fluid (VOF) technique to solve the multiphase flow. The fluid proportions in a computational mesh cell (volume fractions) are defined using this technique. The volume fraction is computed using the given equation,

$$\frac{\partial \alpha_w}{\partial t} + \nabla \cdot (\alpha_w U) = 0 \tag{8}$$

where, U is the velocity field composed of u, v, and w components and α_w is the volume fraction of water, ranging from 0 to 1, with a null value depicting an air filled cell and value of unity representing water filled cell.

The density of the mixture within a mesh cell, required to solve the N-S equations is determined by the volume fraction as follows,

$$\rho = \alpha_w \rho_w + (1 - \alpha_w)\rho_a \tag{9}$$

where, ρ_w and ρ_a are the densities of water and air respectively.

3.3. Stokes second-order wave theory

The degree of accuracy in modelling the generation of ocean waves at the inlet wave and across the domain length is critical to be ensued. With the Ursell number being less than 100 as is the case in the present study, Stokes second-order wave theory is apt and the waves modelled are proved to be sufficiently realistic. The theoretical free surface elevation (η) of waves as per Stokes second-order wave theory is given by,

$$\eta(x,t) = a\{cos\,\theta + ka\frac{3-\sigma^2}{4\sigma^3}cos\,2\theta\}$$
$$\sigma = tanh(kh) \tag{10}$$
$$\theta(x,t) = kx - \omega t$$

where, a is first order wave amplitude, k is the wave number $\left(\frac{2\pi}{\lambda}\right)$, x is the horizontal co-ordinate, ω is the angular frequency $\left(\frac{2\pi}{T}\right)$, T is the time period and h is the mean water depth.

4. Wave generation and WEC-rotor response validation

The model WEC-rotor is to be analyzed with the intent of assessing its hydrodynamic performance and to estimate its power absorption capabilities. Initially, a NWT is modelled and simulated without the WEC rotor to validate the behaviour and propagation of ocean waves. The waves are generated using the inlet velocity method, governed by Stokes second-order wave theory for shallow, intermediate waves. There lies a close agreement in the theoretical and simulated surface elevation profiles. Further, the WEC-rotor is incorporated into the NWT for primarily validating its response to the incoming waves. The results are found to qualitatively match with those of Poguluri et al. [2]. The pitch type rotor may then hold suitable for its performance evaluation. The simulations and analyses discussed are performed using the commercial CFD software, Ansys FLUENT 2020 R2. The NWT is primarily simulated without the WEC rotor so as to accurately model the wave propagation. The set-up and details pertaining to the NWT simulation is discussed herewith.

4.1 NWT without WEC-rotor

For the wave tank modelled, the mean free surface level is set at a height of 3.636 m. The NWT has a domain length of 18.5 m., with coarser grid near the outlet to mitigate reflection from the boundary and interference with upstream waves.

The computational mesh is created using the Ansys meshing tool. A face meshing has been adopted to create a uniformly structured mesh, with edge sizing specified to divide the domain and specify the mesh parameters. A mesh with a higher resolution (0.067 m. x 0.083 m.) is created at the free surface and the beach to capture the waves effectively. The computational uniform mesh for the NWT geometry is shown in Figure 1.

At the inlet of the wave tank, inlet velocity method is adopted using Stokes second-order wave theory, with wave conditions specified as following (Table 2). At the top, an atmospheric outlet is specified allowing air to flow across the boundary. The bottom is specified to be a wall with a no slip shear condition. Lastly, the outlet is to have a free surface level of 3.636 m subjected to pressure outlet.

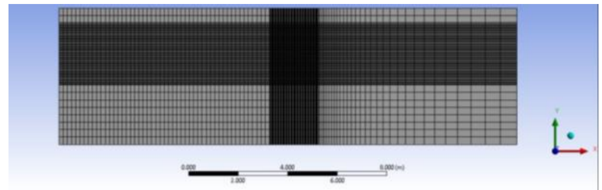

Figure 1: Computational mesh for the NWT geometry

The VOF formulation is explicitly marched. A piecewise-linear technique is used to depict the interface between fluids in the geometric reconstruction scheme. Comparative studies on the effects of turbulence on the wave behavior reveal the results to be invariable in comparison with laminar flow. Thus, a laminar viscous model is used for this study. Second order upwind and body force weighted schemes are used for momentum and pressure discretization respectively. To enhance computation, the pressure-implicit with splitting of operators (PISO) scheme is considered in order to perform neighbor and skewness corrections.

Table 2: Wave parameters specified at inlet of NWT

Wave height	Wavelength	Wave period	Water depth
0.136 m.	4.78 m.	1.75 sec.	3.636 m

The accuracy in results achieved is based on the comparison between the theoretical and simulated profiles of surface elevation. The water volume fraction contour at a sample time of t=30 sec. is shown in Figure 2. This offers an insight on the propagation of waves from the inlet specified across the length of the domain, till the beach. The surface elevation profiles across the length of the NWT for different time intervals are depicted in Figures 3–5. The theoretical and simulated profiles are found to lie in close agreement. However, mismatches in the profiles at the wave crests and troughs are mainly attributed to the interference of a part of the reflected waves with the waves generated. It can be seen as an indication of the coarser grid near the outlet being ineffective in dampening the waves upstream. Techniques for enhancing the prevention of wave reflection include control over simulation time, creating a porous damping zone or increasing the domain length further.

Figure 2: Water volume fraction contour at a sample time of t=30 sec

The inlet velocity approach specified using higher order Stokes wave theories could be explored, with the prospects of improved results over those depicted. This however comes at the expense of greater computation times. Moreover, an alternative to generate the waves using the piston-type wave maker may allow control over simulation time to prevent reflection of waves at the boundary. This would aid to establishing simulated results having a better agreement with the theoretical profiles.

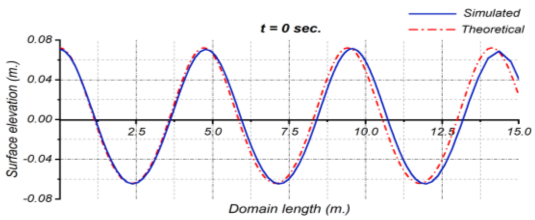

Figure 3: Theoretical and simulated surface elevation at t=0 sec

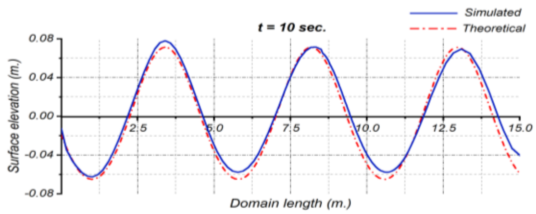

Figure 4: Theoretical and simulated surface elevation at t=10 sec

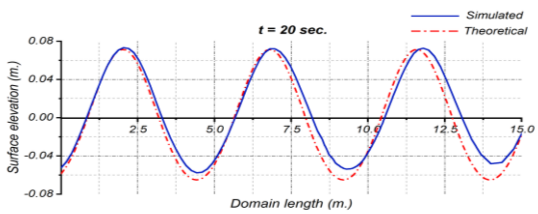

Figure 5: Theoretical and simulated surface elevation at t=20 sec

4.2 NWT with WEC- rotor

A Salter's duck rotor has been considered for the present study. The paunch of the rotor replicates the fluid particle displacement. The wave dynamic pressure forces the rotor to pitch about its axis. The stern of the rotor is almost circular and does not reflect waves on the leeward side. The WEC-rotor is constrained to have a single degree of freedom rotary motion and the various parameters viz angular velocity, pitch response and power absorption are to be evaluated over time for a set of sea states. The system response has been studied without considering the effects of power take-off. The schematic of WEC-rotor with some of its features labelled is shown in Figure 6. The WEC-rotor geometry is scaled with a Froude's factor of 11 (scale factor limits to 50 for short wave conditions as per Hughes [6]), the model data recorded in Table 3. The dimensional figures are adopted from the works of Poguluri et al. [2] for the validation of WEC-rotor response and further simulations for performance assessment. The set-up and details pertaining to the simulation of NWT in the presence of WEC-rotor is discussed in the subsequent sub-sections.

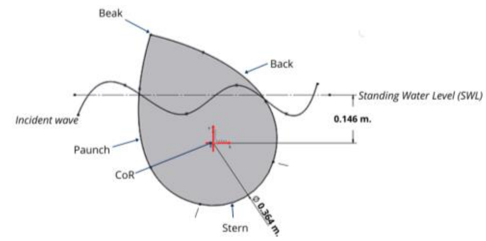

Figure 6: Schematic of model WEC-rotor

Table 3: Full-scale and model data of wave and WEC-rotor parameters

	Full scale data	Model data (1:11)
Wave parameter		
Wave height (m.)	1.5	0.1364
Wave period (s)	5.764	1.738
Wavelength (m.)	51.741	4.704
Water depth (m.)	40	3.636
WEC-rotor parameter		
Stern diameter (m.)	4	0.364
Depth of submergence (m.)	3.6	0.327
Beak angle (^{o})	60	60
Total mass (kg)	18168.15	13.65
Pitch moment of inertia about CoR (kg.m^2)	120450.04	0.7479
Horizontal CG w.r.t CoR (m.)	-1.0241	-0.0931
Vertical CG w.r.t CoR (m.)	1.0978	0.0998

The set-up geometry is shown in Figure 7. The geometry and meshing details for the background is as discussed. As for the WEC-rotor, a radial overset component mesh zone of 1.6 m. diameter is created encircling it (refer Figure 8).

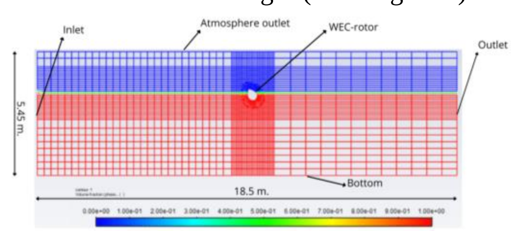

Figure 7: Geometry of Numerical Wave Tank (NWT) with WEC-rotor

The overset mesh superimposed on the background mesh ensures the needed data interpolation across these zones. A bias specified along the radial direction of the component mesh zone offers greater refinement at the rotor boundaries. Along the circumferential direction the grid is equispaced. The overset mesh has an orthogonal quality tending to unity (0.99).

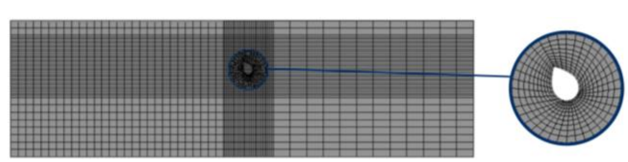

Figure 8: Computational mesh for the NWT geometry with WEC-rotor - a magnified view of the overset mesh depicted

Additionally, the component mesh zone boundary is specified as an overset, while the WEC-rotor boundary is considered to be a wall with no slip shear condition. The solution methods and controls adopted for the NWT simulations in the presence of WEC-rotor are modified to an extent in comparison with those in its absence. The VOF formulation is implicitly marched with the transport equation not to be solved iteratively for every time step. With regard to spatial discretization, the compressive volume fraction discretization scheme proves to depict improvised results over modified HRIC. The free surface is considered flat initially.

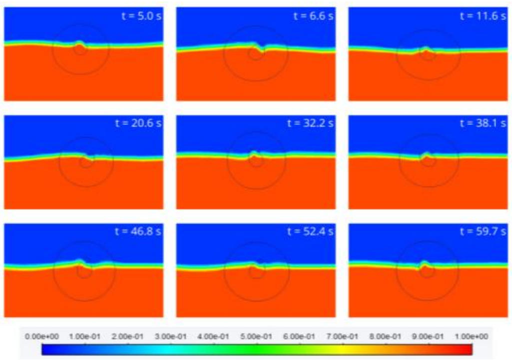

Figure 9: WEC-rotor response to waves of H_s = 1.5 m. and T_e = 5.76 s at different time stamps

Based on the simulations performed, the pitch type motion of the WEC-rotor can be identified from the snap views shown in Figure 9 at different time stamps. The motion of the rotor is found to be synchronizing with that of the incident waves, i.e., the rotor attains its mean position as the wave peak to its maximum height. As the waves strike the rotor boundary the amplitude of the wave is diminished aft of the rotor.

The angular velocity variation and pitch response of the WEC-rotor have been plotted (refer Figure 10 and Figure 11). The patterns are found to closely resemble those of isolated WEC-rotors without considering PTO in the works of Poguluri et al. [2]. The angular velocity gradually builds up over time and attains a nearly constant value. The plots could be verified by observing the complementary nature of angular velocity and pitch response. The peak angular displacement lags by nearly 1.44 sec with respect to peak angular velocity of corresponding cycle. It is worthwhile to note that though the patterns are similar, the amplitude of angular velocity and pitch response seem under predicted. This could be attributed to restricting the simulations to a 2D domain, which fails to consider diffusion of waves across the rotor faces along the third dimension. This can cause further amplification or attenuation of profiles (see Figure 10(b) and Figure 11(b)).

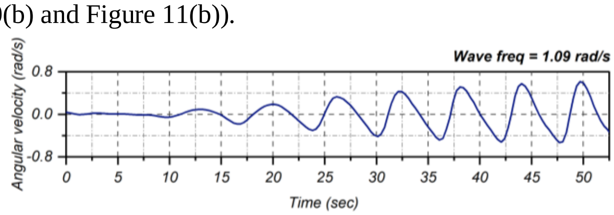

(a)

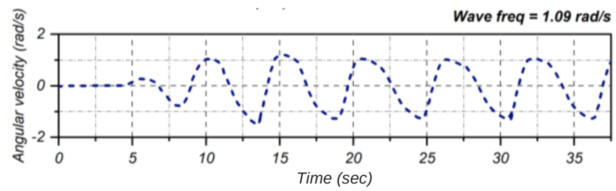

(b)

Figure 10: Angular velocity variation of WEC-rotor over time for wave frequency of 1.09 rad/s (a) Fluent simulation (b) Poguluri et al.

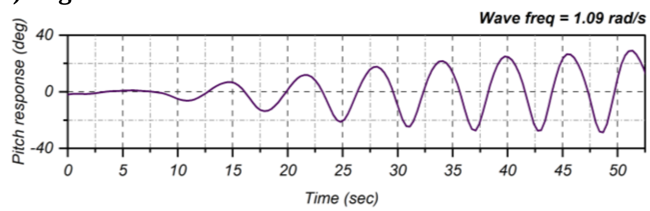

(a)

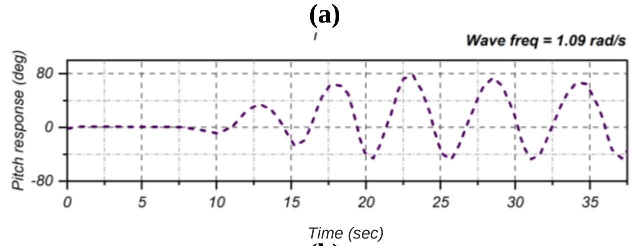

(b)

Figure 11: Pitch response of WEC-rotor for wave frequency of 1.09 rad/s (a) Fluent simulation (b) Poguluri et al.

5. Study of WEC-rotor behaviour in selected sea-states

The WEC-rotor performance is assessed for different sea-states (i.e., for different wave frequencies) of relatively higher probabilities of occurrence at the selected site, Karwar. This assessment is necessary in order to determine the feasibility of the rotor. The rotor power absorption capability followed by the efficiency of the rotor for each sea state is calculated and compared. The following sea-states are taken from the scatter diagram for the study (refer Table 4).

Table 4: Sea States considered for study of rotor assessment

Sea-state	Wave Height (m)	Time Period (s)
I	1.0	5.0
II	1.0	6.0
III	1.5	6.0
IV	2.0	6.0

Two sample sets of resultant plots for angular velocity and pitch response of the WEC-rotor for each of the sea-states analyzed are shown herewith (refer Figure 12 and Figure 13).

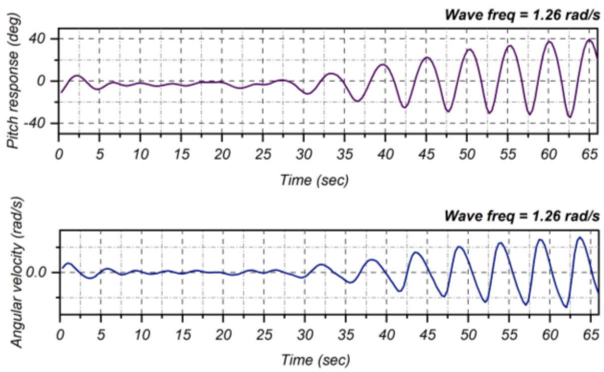

Figure 12: Angular velocity and pitch response variation of WEC-rotor for H_s = 1.0 m. and T_e = 5 sec

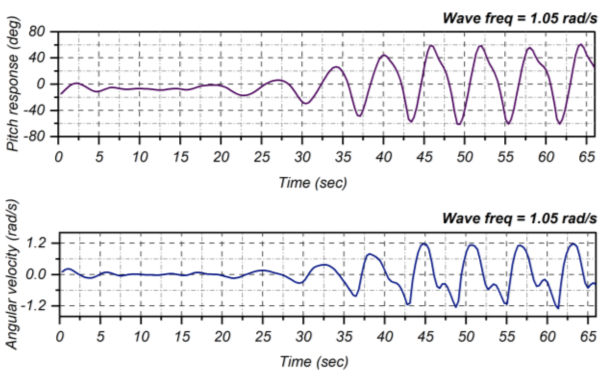

Figure 13: Angular velocity and pitch response variation of WEC-rotor for H_s = 1.5 m. and T_e = 6 sec

It may be observed that as wave height increases there is a surge in the angular acceleration of the rotor, as a result of which the power absorption trivially increases. At certain time periods of the waves, minor distortions in the angular displacement profiles are notable. This is majorly due to the wave frequency being far from the natural frequency of the rotor. From the angular velocity data, the angular acceleration is obtained over time, considering minor increments of flow time. The power absorbed results in the acceleration of the WEC-rotor, while a part of it is dissipated due to viscous and PTO damping. Considering the power component causing acceleration to dominate, the average power absorption over the time stretch is computed and is given by. The results obtained by this are recorded below in Table 5.

$$< P_a >= \frac{\int (I w_R \alpha_R) dt}{T} \tag{11}$$

The hydrodynamic efficiency of WEC-rotor would then be given as,

$$\acute{\eta}_H = \frac{< P_a >}{P_w} * 100\% \tag{12}$$

While there is an increase in the power absorption as the waves get stronger, there is a decrease in hydrodynamic efficiency of the WEC-rotor identified. This is owed to a failure in attaining the resonance condition.

Table 5: Power absorption and hydrodynamic efficiency at different sea-states

Sea-state	Power absorption (kW)	Incident power (kW)	Hydrodynamic efficiency
I	9.916	12.371	80.15%
II	13.282	14.846	89.47%
III	23.652	33.403	70.81%
IV	30.601	59.383	51.53%

6. SUMMARY OF RESULTS

The present work discusses approaches involved in selection of optimal site for ocean wave energy harnessing based on comparison of indices. Based on an ideal mechanism chosen for the selected site, the Salter's duck WEC-rotor is considered for CFD investigations. For analysis, a numerical wave tank is first developed, with wave generation is specified using the Stokes second-order wave theory. The results show a close agreement between the theoretical and simulation surface elevation profiles. Subsequently, while the WEC-rotor is incorporated into the NWT, Froude's scaling is used to ensure dynamic parallels amidst actual and simulation results.

The response of the pitch type WEC-rotor has been qualitatively validated against the results of Poguluri et al. [2]. The scatter diagram for the wave energy resource at the selected site, Karwar is used to for the selection of sea-states in the vicinity of the ones of suitable occurrence. Based on the simulations carried out, the average power absorption capacity and hydrodynamic efficiency of the WEC-rotor are computed. Although the power absorption increases as the waves strengthen, a decrease in hydrodynamic efficiency of the WEC-rotor occurs due to the wave frequency being much deviated from the natural frequency of the rotor.

7. CONCLUSIONS

With most of the wave energy harnessing mechanisms remaining far from their deployment for commercial use, efforts to make them techno-economically feasible are ongoing and vastly challenging.

- Based on the 4 sea-states considered with increasing incident power for the analysis, the power absorbed by the WEC-rotor is found to proportionally increase. However, the hydrodynamic efficiencies are roughly 80%, 89%, 70% and 51% for the respective sea-states.
- The present study incorporates a two-dimensional NWT for the assessment, but a CFD based three-dimensional NWT may be preferable to study the hydrodynamics of a pitching type WEC-rotor with incident regular waves.
- Moreover, a more realistic approach would be to consider irregular waves as those incident on the device are not always linear. The study also reveals the importance in dealing with PTO damping and its effects on the energy harnessing device.

- Besides, the WEC-rotor must be suitably designed such that it resonates with the wave field using control systems. Some of the recent technological developments include control strategies that bring variation in PTO damping through continuous monitoring of the incident waves to optimize the power absorption.

ACKNOWLEDGEMENTS

The authors are grateful to Earth System Science Organization - Indian National Centre for Ocean Information Services (ESSO – INCOIS), Ministry of Earth Sciences, Government of India for providing the oceanographic information for the wave resource assessment through Wave Rider Buoy (WRB) measurements.

REFERENCES

[1] Raju VS, Ravindran M. Wave energy: potential and programme in India. Renewable energy. 1997 Feb 1;10.

[2] Poguluri SK, Kim D, Bae YH. Hydrodynamic Analysis of a Multibody Wave Energy Converter in Regular Waves. Processes. 2021 Jul;9(7):1233.

[3] Lavidas G. Selection index for Wave Energy Deployments (SIWED): A near-deterministic index for wave energy converters. Energy. 2020 Apr 1;196:117131.

[4] Kamranzad B, Etemad-Shahidi A, Chegini V. Developing an optimum hotspot identifier for wave energy extracting in the northern Persian Gulf. Renewable Energy. 2017 Dec 1;114:59-71.

[5] Zubiate L, Villate JL, Torre-Enciso Y, Soerensen HC, Holmes B, Panagiotopoulos M, Neumann F, Rousseau N, Langston D. Methodology for site selection for wave energy projects. In8th European Wave and Tidal Energy Conference, Uppsala, Sweden 2009 Sep.

[6] Hughes SA. Physical models and laboratory techniques in coastal engineering. World Scientific; 1993 Nov 26.